

Recent Climatology, Variability, and Trends in Global Surface Humidity

AIGUO DAI

National Center for Atmospheric Research, Boulder, Colorado*

(Manuscript received 20 July 2005, in final form 22 November 2005)

ABSTRACT

In situ observations of surface air and dewpoint temperatures and air pressure from over 15 000 weather stations and from ships are used to calculate surface specific (q) and relative (RH) humidity over the globe (60°S–75°N) from December 1975 to spring 2005. Seasonal and interannual variations and linear trends are analyzed in relation to observed surface temperature (T) changes and simulated changes by a coupled climate model [namely the Parallel Climate Model (PCM)] with realistic forcing. It is found that spatial patterns of long-term mean q are largely controlled by climatological surface temperature, with the largest q of 17–19 g kg⁻¹ in the Tropics and large seasonal variations over northern mid- and high-latitude land. Surface RH has relatively small spatial and interannual variations, with a mean value of 75%–80% over most oceans in all seasons and 70%–80% over most land areas except for deserts and high terrain, where RH is 30%–60%. Nighttime mean RH is 2%–15% higher than daytime RH over most land areas because of large diurnal temperature variations. The leading EOFs in both q and RH depict long-term trends, while the second EOF of q is related to the El Niño–Southern Oscillation (ENSO). During 1976–2004, global changes in surface RH are small (within 0.6% for absolute values), although decreasing trends of $-0.11\% \sim -0.22\%$ decade⁻¹ for global oceans are statistically significant. Large RH increases (0.5%–2.0% decade⁻¹) occurred over the central and eastern United States, India, and western China, resulting from large q increases coupled with moderate warming and increases in low clouds over these regions during 1976–2004. Statistically very significant increasing trends are found in global and Northern Hemispheric q and T . From 1976 to 2004, annual q (T) increased by 0.06 g kg⁻¹ (0.16°C) decade⁻¹ globally and 0.08 g kg⁻¹ (0.20°C) decade⁻¹ in the Northern Hemisphere, while the Southern Hemispheric q trend is positive but statistically insignificant. Over land, the q and T trends are larger at night than during the day. The largest percentage increases in surface q ($\sim 1.5\%$ to 6.0% decade⁻¹) occurred over Eurasia where large warming ($\sim 0.2^\circ$ to 0.7°C decade⁻¹) was observed. The q and T trends are found in all seasons over much of Eurasia (largest in boreal winter) and the Atlantic Ocean. Significant correlation between annual q and T is found over most oceans ($r = 0.6$ – 0.9) and most of Eurasia ($r = 0.4$ – 0.8), whereas it is insignificant over subtropical land areas. RH– T correlation is weak over most of the globe but is negative over many arid areas. The q – T anomaly relationship is approximately linear so that surface q over the globe, global land, and ocean increases by $\sim 4.9\%$, 4.3% , and 5.7% per 1°C warming, respectively, values that are close to those suggested by the Clausius–Clapeyron equation with a constant RH. The recent q and T trends and the q – T relationship are broadly captured by the PCM; however, the model overestimates volcanic cooling and the trends in the Southern Hemisphere.

1. Introduction

Atmospheric water vapor provides the single largest greenhouse effect on the earth's climate. All climate

models predict increased atmospheric content of water vapor with small changes in relative humidity as the global-mean surface temperature rises in response to increased CO₂ and other greenhouse gases (Cubasch et al. 2001; Dai et al. 2001). The increased water vapor provides the single largest positive feedback on surface temperature (Hansen et al. 1984) and is the main cause of increased precipitation at mid- and high latitudes in the model simulations. It is therefore vital to monitor changes in atmospheric water vapor content not only for detecting global warming but also for validating the large water vapor feedback seen in climate models.

* The National Center for Atmospheric Research is sponsored by the National Science Foundation.

Corresponding author address: A. Dai, National Center for Atmospheric Research, P.O. Box 3000, Boulder, CO 80307-3000.
E-mail: adai@ucar.edu

Atmospheric water vapor has been traditionally observed by balloon-borne radiosondes (for relative humidity) at about 700–800 land stations, mostly in the Northern Hemisphere (Wang et al. 2000). The sounding data show increasing water vapor trends exceeding 3% per decade during 1973–95 over most of North America, east China, and some islands in the western tropical Pacific (Ross and Elliott 2001). However, because of their poor spatial sampling (e.g., no soundings over open oceans) and temporal inhomogeneities due to changes in radiosonde sensors (Elliott 1995; Wang et al. 2002), radiosonde measurements of atmospheric humidity are insufficient for estimating changes in global atmospheric water content during recent decades. Other atmospheric water vapor products often contain major problems, although satellite [Special Sensor Microwave Imager (SSM/I)] observations reveal an increase of $1.3\% \pm 0.3\%$ per decade in atmospheric precipitable water (PW) for the ocean as a whole from 1988 to 2003, which is strongly related to sea surface temperature (SST) increases (Trenberth et al. 2005).

At the surface, water vapor (or humidity) is an important meteorological and climate variable that affects human comfort (Changnon et al. 2003), surface evaporation and plants' transpiration. Surface specific (q) and relative humidity (RH) is conventionally measured using wet and dry bulb thermometers or RH sensors exposed in thermometer screens at a large number of weather and climate stations and on many marine platforms. The measurements of dewpoint temperatures (T_d) by dew cells usually have an accuracy of about $\pm 0.5^\circ\text{C}$ (Brock 1984; Brock and Richardson 2001), and it is lower ($\pm 1.5^\circ\text{C}$) in very cold conditions ($T_d < -10^\circ\text{C}$) (Déry and Stieglitz 2002). Some surface stations and buoys use RH-based sensors to measure RH directly. The synoptic datasets used here contain a dewpoint temperature, which may be derived from different types of humidity measurements (but most often from dry and wet bulb temperatures). The quality of the humidity measurements can be contaminated by local environments (e.g., heating, ventilation, etc.) and may be affected by a lack of calibration (Brock and Richardson 2001; Déry and Stieglitz 2002). An analysis of Canadian surface humidity records (van Wijnngaarden and Vincent 2005) shows that many major instrumental changes occurred at Canadian stations, mostly before the mid-1970s (i.e., before the data period of this study). Nevertheless, these humidity measurements have been widely used to derive surface humidity climatologies and changes (see below) mainly because these are the only in situ observations available over most of the globe.

The surface observations provide much better spatial

and temporal sampling than radiosondes. Because water vapor in the lower troposphere is generally well mixed and the lower troposphere accounts for the majority of atmospheric total water content, variations in surface q , especially on weekly and longer time scales, are found to strongly correlated with atmospheric PW (Reitan 1963; Bolsenga 1965; Liu 1986; Liu et al. 1991). In fact, Smith (1966) derived a power relationship (over both land and oceans) between surface specific humidity q_o at pressure level p_o and atmospheric q at pressure level p : $q/q_o = (p/p_o)^\lambda$, where parameter λ varies with latitudes and seasons within a range of about 1.11–3.50 (Smith 1966; Liu et al. 1991). These studies suggest that historical records of surface q , which has near-global sampling, can provide useful information on changes in atmospheric water vapor content, especially over the oceans where upper-air soundings have been unavailable.

Long-term mean distributions of surface q over the globe (Oort 1983); RH over the oceans (Trenberth et al. 1989; Peixoto and Oort 1996); and q , RH, and T_d over the United States (Gaffen and Ross 1999) have been studied using the surface humidity observations. These studies show large seasonal and spatial variations in surface q , while the variations in surface RH are relatively small over the oceans but considerable over the United States. Surface humidity fields are also produced by atmospheric reanalyses, but they usually make no use of surface observations and thus may contain biases.

There are a number of regional analyses of historical changes in surface water vapor content over land. For example, increased surface dewpoint temperature and specific humidity over the contiguous United States during the second half of the twentieth century have been reported by several studies (e.g., Gaffen and Ross 1999; Robinson 2000; Sun et al. 2000; Groisman et al. 2004). During the same period, increased surface water vapor content is also found over Europe (Schönwiese and Rapp 1997; New et al. 2000; Philipona et al. 2004), the former Soviet Union, eastern China, tropical western Pacific islands (Sun et al. 2000), and China (Kaiser 2000; Wang and Gaffen 2001). Positive trends from 1975 to 1995 in surface vapor pressure are also found over a few other regions such as Alaska, western Canada, and Japan (New et al. 2000). Over the oceans, Ishii et al. (2005) show that global-mean oceanic dewpoint temperature has risen by about 0.25°C from 1950 to 2000. Most of the previous studies cover only a fraction of the globe and do not include the data of the last 5–15 yr. Furthermore, trends in dewpoint temperature and vapor pressure may differ from humidity because q is a nonlinear function of air pressure and dewpoint

temperature while vapor pressure varies with both air pressure and q (see section 2). Thus a global view of surface humidity (i.e., q and RH) changes during the most recent decades has been unavailable.

Here we analyze surface q and RH derived using surface 3-hourly observations from over 15 000 weather stations over global land and marine reports from ships and buoys over global oceans from December 1975 to spring 2005. We first produce a seasonal climatology of surface q and RH and examine their year-to-year variability, and then analyze their trends and the association with recent warming. We focus on the most recent decades when global-mean surface temperature has been rising rapidly (Jones and Moberg 2003) and surface observations have a much better spatial coverage than earlier periods. For comparison, we also analyze recent humidity changes and their relationship with temperature simulated by a fully coupled climate system model. Our results update previous climatologies of surface humidity and provide a first near-global assessment of changes in surface water vapor content and relative humidity in association with recent global warming. We emphasize that humidity is one of the most difficult basic meteorological variables to measure (Brock and Richardson 2001). As such, considerable instrumental and sampling errors likely exist in the data despite our data quality control efforts. Nevertheless, we believe that the q and RH results reported here (including the trends) are likely reliable, at least in a qualitative sense, as suggested by the strong q -temperature correlations.

In section 2, we first describe the datasets and analysis procedures. We then discuss the mean patterns, seasonal to interannual variations, and empirical orthogonal function (EOF) analyses in section 3. The trends in surface RH and q , their association with surface temperature increases, and comparisons with twentieth-century climate simulations by a coupled model are described in section 4. A summary is given in section 5.

2. Datasets and analysis procedures

The datasets used in this study are summarized in Table 1. We calculated 3-hourly, instantaneous surface specific q and RH from 1 December 1975 to 30 April 2005 (31 May 2005 over the oceans) using individual synoptic reports of surface air and dewpoint temperatures and air pressure from over 15 000 weather stations and marine reports from ships around the globe (buoys usually do not measure Td). Both the station and marine synoptic weather reports were transmitted in real time through the Global Telecommunication Systems (GTS) and archived at the National Center for Atmo-

TABLE 1. Datasets used in this study. The time period is the period examined in this study. Tair, Td, Ps, and q are surface air temperature, dewpoint temperature, air pressure, and specific humidity, respectively. Surface q and RH were derived from Tair, Td, and Ps.

Variables	Dataset name	Coverage, resolution	Time period	Source or references
Tair, Td, Ps	DS464.0	Global, ~15 000 stations, plus ships; 3 hourly	1 Dec 1975–30 Apr 2005	NCAR; http://dss.ucar.edu/datasets/ds464.0/
Tair, Td, Ps	ICOADS	Oceanic, ships; 3 hourly	1 Dec 1975–31 Dec 2002	NOAA; http://www.cdc.noaa.gov/coads/
Tair, Td, Ps	ICOADS real-time data	Oceanic, ships; 3 hourly	1 Jan 2003–31 May 2005	NOAA; http://www.cdc.noaa.gov/coads/nrt.html
Tair (land), SST (ocean)	HadCRUT2	Global, 5° × 5°; monthly	Dec 1975–Mar 2004	CRU; Jones and Moberg (2003); Rayner et al. (2000)
Tair, q	PCM twentieth-century runs	Global, 2.8° × 2.8°; monthly	Dec 1975–Dec 1999	NCAR; Meehl et al. (2004)
Cloud cover	Surface, obs	Global, stations; 3 hourly	1 Dec 1975–30 Apr 2005	NCAR, NOAA NCDC; Dai et al. (2006)

spheric Research (NCAR) from 1975 (incomplete for 1975) to present (DS464.0; see <http://dss.ucar.edu/datasets/ds464.0/>). The marine GTS weather reports, supplemented by other sources of data, were also used to compile and produce the quality-controlled International Comprehensive Ocean–Atmosphere Data Set (ICOADS; Worley et al. 2005; <http://www.cdc.noaa.gov/coads/>), which was also used here to calculate instantaneous surface q and RH. The ICOADS ends on 31 December 2002; thereafter, we calculated marine surface q and RH using the synoptic reports from the DS464.0 dataset, which includes all the marine reports in the GTS, and also the real-time marine reports from the ICOADS project (see <http://www.cdc.noaa.gov/coads/nrt.html>) if data were unavailable from the DS464.0 for a given ocean box (see below).

These surface synoptic reports are the primary in situ observations of the weather and climate. They have provided the basic instrumental data used to compile global monthly temperature and other climate records that have been applied in numerous studies, for example, to document the historical changes in global surface temperature (e.g., Hansen et al. 2001; Jones and Moberg 2003) and cloud cover (e.g., Norris 2005; Dai et al. 2006) and to quantify variability in surface pressure tides (Dai and Wang 1999), surface winds and divergence (Dai and Deser 1999), precipitation and thunderstorm frequencies (Dai 2001a,b), and cloud amount (e.g., Warren et al. 1988).

The individual reports of surface air (T ; in $^{\circ}\text{C}$) and dewpoint (T_d ; in $^{\circ}\text{C}$) temperatures and surface air pressure (P_s ; in mb) were first screened to be within a broad, physically possible range, namely, -80°C for T_a and T_d and 200–1200 mb for P_s . These data were then averaged over each 1° grid box, and the mean and standard deviation (for individual reports relative to the grid box mean) were computed for each season for the whole data period. This standard deviation (s.d.) was used to exclude outliers locally. Tests showed that using a criterion of either 3.0 or 4.5 s.d. yielded similar results. However, because of the nonstationary nature of the data time series of the last 30 yr, a tight range (e.g., 3 s.d.) excludes more data points in the early and late years of the data period than in other years, which results in reduced magnitudes of the trends in the data. To be consistent with the ICOADS, data points outside the ± 4.5 s.d. range were excluded for both the DS464.0 and ICOADS datasets, which generally reduced the magnitude of the trends only slightly compared to the case without this screening.

The screened data were used to calculate q (g kg^{-1}) according to (Oort 1983, p. 20)

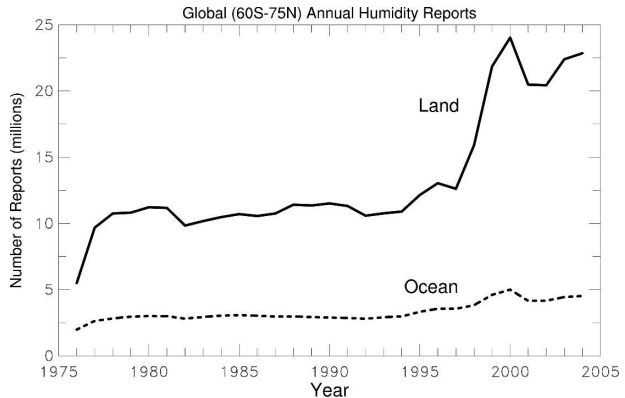


FIG. 1. Time series of annual total number of surface specific humidity observations derived from reports of surface air and dewpoint temperature and air pressure from weather stations over global (60°S – 75°N) land (solid curve) and from ships (dashed curve).

$$q = 622 \frac{6.11}{P_s} 10^{\frac{7.5T_d}{T_d+237.3}} \quad (1)$$

and RH (%) using

$$RH \equiv 100 \frac{w}{w_s}, \quad w \equiv \frac{q}{1000 - q}, \quad w_s \equiv \frac{0.622e_s}{P_s - e_s}, \quad (2)$$

where the saturation vapor pressure e_s (in mb) is calculated according to (Bolton 1980)

$$e_s = 6.112e^{\frac{17.67T}{T+243.5}}. \quad (3)$$

The calculated q and RH were also subjected to a range check (0%–100% for RH and 0–99 g kg^{-1} for q) and similar s.d.-based screening. The above quality checks were intended to exclude outliers that likely result from errors in measurements, data transmission, and other sources. Remaining random errors in the T , q , and RH data are greatly reduced during the averaging to derive gridded seasonal mean values because the number of samples is large over most regions (cf. Figs. 1–2). No attempt was made here to address potential systematic errors and biases that might result from changes in ship heights, instrumentation, and other factors because metadata for these changes are currently unavailable and statistical tests for nonclimatic changes without any metadata are not very effective for a relatively short length of records.

The screened instantaneous q and RH values were first simply averaged within each 1° latitude \times 1° longitude land box and $4^{\circ} \times 5^{\circ}$ ocean box for each season and then averaged over December 1975–November 2004 to create a long-term seasonal climatology, which is used in section 3 for describing the spatial and seasonal variations. The instantaneous q and RH (and T)

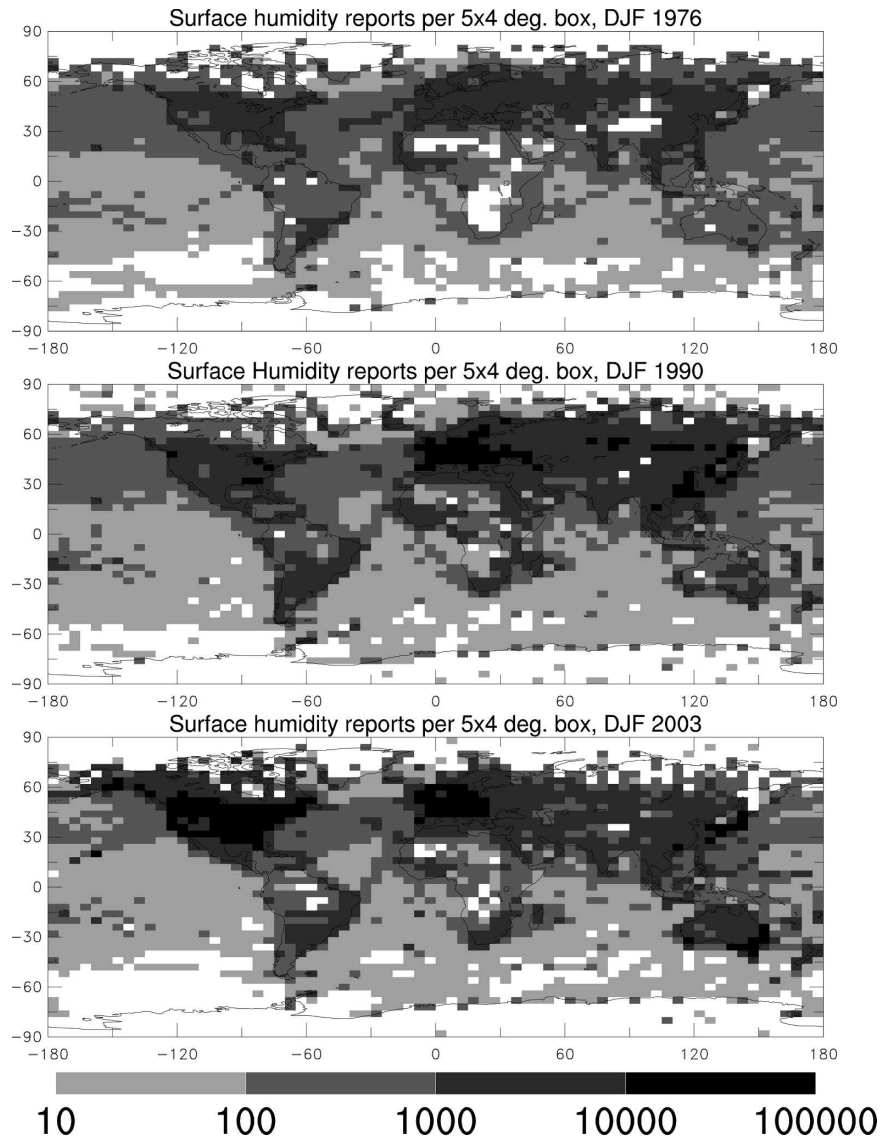


FIG. 2. Number of specific humidity observations per each 4° lat \times 5° lon box during DJF for year (top) 1976, (middle) 1990, and (bottom) 2003. Blank areas have less than 10 observations.

data were then processed again, in which they were stratified by the observation time (0000, 0300, 0600Z, etc.) from which seasonal mean values were computed (so that diurnal sampling biases were minimized), averaged for each individual seasonal and within each $1^{\circ} \times 1^{\circ}$ land box and $4^{\circ} \times 5^{\circ}$ ocean box, subtracted from the climatologic mean, and the anomalies were averaged (for land boxes) to a $4^{\circ} \times 5^{\circ}$ global grid. The gridded seasonal anomalies were used to compute the standard deviation, EOFs, and long-term trends. The use of the anomalies minimizes the effect of changing sampling (e.g., over regions with large differences in the mean) on area-weighted regional and global time se-

ries. Linear regression was used to estimate the trends and Student's t tests were used to test the statistical significance of the trends of the humidity and temperature time series.

Local solar heating effects on daytime T measured onboard ships and from buoys can be large (up to $\sim 3^{\circ}\text{C}$) in calm and sunny days, and their corrections are complicated and require ship or buoy-specific coefficients (Anderson and Baumgartner 1998; Berry et al. 2004). Fortunately, the solar heating effect on q is negligible (less than 0.1 g kg^{-1}) when q is calculated using the measured (i.e., uncorrected) T and T_d (Kent and Taylor 1996). Our results show little day–night differ-

ence in marine q ($\sim 0.2\text{--}0.5\text{ g kg}^{-1}$ at low latitudes and smaller at higher latitudes), which is consistent with Kent and Taylor (1996). To avoid the local heating effect on marine surface air temperature, we used SST over the oceans (and air temperature over land) for oceanic T change analyses, similar to the Hadley Centre and Climate Research Unit temperature dataset (HadCRUT2; see Jones and Moberg 2003; Rayner et al. 2003). For climatological and diurnal analyses of RH, the heating bias in marine air temperature could have significant impacts [through Eqs. (2)–(3)]. We corrected the heating bias in surface air temperature from ships using the method of Kent et al. (1993) for ICOADS data for 1976–2002. However, we were unable to do the correction for years after 2002 because ship movement data (needed for the correction) were unavailable in the other datasets. The correction changes the T and RH diurnal cycle greatly but has small effects on their interannual to longer-term variations. Thus we used the corrected marine air temperature for the 1976–2002 RH climatology, s.d., and diurnal analysis, but used the uncorrected marine air temperature for the RH anomaly and change analysis for 1976–2004 (in order to be consistent for the whole data period). We found that over the oceans seasonal and annual q correlates more strongly with accompanying surface air temperature than with SST. Tests showed that the correction for solar heating bias has little effect on the seasonal and annual q – T relationships. Thus we used the uncorrected marine air temperature for the whole data period (1976–2004) in the q – T scatterplots and correlative analyses.

Figure 1 shows the time series of annual total number of weather reports that can be used to derive valid q values using Eq. (1) over the global (60°S – 70°N) land (solid curve) and from ships (dashed curve). The number of observations over land is relatively stable (~ 10 – 13 million yr^{-1}) from 1977 to 1997; thereafter it increased to ~ 20 – 23 million yr^{-1} mainly because of the inclusion of a large number of hourly reports from the United States and other regions (cf. Fig. 2). We included these hourly reports in the nearest 3-hourly averages (e.g., 01 UTC reports were included in the averaged values for 00 UTC). Figure 2 shows that the seasonal number of q samples for each $4^{\circ} \times 5^{\circ}$ grid box is large (10^3 – 10^5) over most land areas and probably adequate (10^2 – 10^3) over the North Atlantic and North Pacific Oceans, but the sampling (<100) is poor over many tropical and southern oceans. Observations over Africa and the Amazon are also relatively sparse.

For comparison, surface q and T for 1976–99 from four ensemble twentieth-century climate simulations by a coupled climate system model, namely the Parallel

Climate Model (PCM) (Washington et al. 2000), were also analyzed. The PCM has a horizontal resolution of $\sim 2.8^{\circ}$ and 18 vertical layers, with the lowest layer centered at a pressure level of $0.9925 \times$ surface pressure. The surface humidity in the model is controlled by a number of processes, including atmospheric circulation, vertical mixing, and surface evaporation, which is affected by wind speed, soil moisture, solar heating, and other factors. The twentieth-century simulations include observed greenhouse gas, sulfate aerosol, ozone, volcanic, and solar forcing; they are designed to reproduce the historical climate changes (see Meehl et al. 2004 for details).

3. Spatial and temporal variations

Figure 3 shows the spatial distribution of long-term mean seasonal q at the surface. Associated with the warm temperatures in the Tropics, the highest values of q (17 – 19 g kg^{-1}) are seen over tropical oceans and land areas. This band of maximum q migrates seasonally in a south–northward direction only slightly. Outside the Tropics, large latitudinal gradients exist on both the hemispheres, together with large seasonal variations over land. For example, over central Asia q varies from ~ 1 – 2 g kg^{-1} in winter to 7 – 8 g kg^{-1} in summer. Longitudinal variations are relatively small, although q over the deserts in northern and southern Africa, the Middle East, and inland Australia is much lower than other places at similar latitudes. This implies drying effects on surface humidity by dry soils and atmospheric subsidence over subtropical land. Excluding these subtropical areas, the spatial patterns of surface q are very similar to those of surface T (e.g., Shea 1986). This suggests that surface T largely controls surface q outside the subtropical land areas through Eq. (3) (note that surface evaporation is proportional to $q_s - q$, where q_s is the saturation specific humidity at the surface).

The December–February (DJF) and June–August (JJA) q maps of Fig. 3 are similar to those shown by Oort (1983, his Fig. A15, for 1963–73), although Fig. 3 shows more details over mid- and high latitudes (mainly due to finer contour levels in Fig. 3). Over the United States, q distributions in Fig. 3 are also comparable with those (for 1961–90) of Gaffen and Ross (1999), who derived q from measurements of RH. For example, they both show 2 – 4 g kg^{-1} in DJF over the central and northern United States and 10 – 17 g kg^{-1} in JJA over the southern central and southeast United States.

The control of surface T on q is also implied by the relatively invariant distribution of surface RH over the oceans. Figure 4 shows that RH is around 75% – 82% over most oceans with relatively small ($\leq 5\%$) seasonal

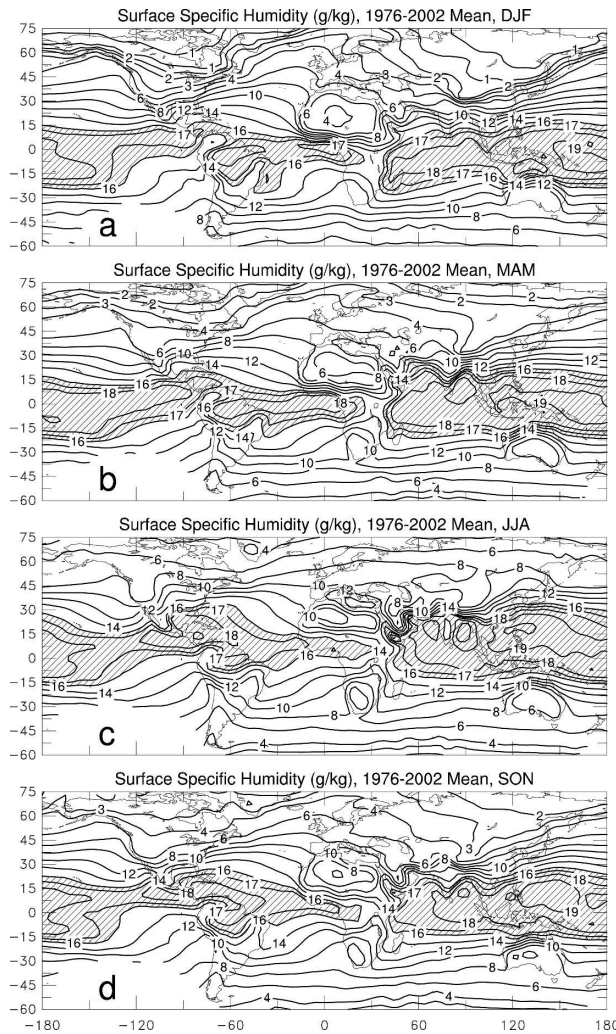


FIG. 3. Long-term (1976–2002) mean surface specific humidity (g kg^{-1}) derived from surface observations for the four seasons: (a) DJF, (b) MAM, (c) JJA, and (d) SON. Contour levels are 0.5, 1, 2, 3, 4, 6, 8, 10, 12, 14, 16, 17, 18, 19, and 20 g kg^{-1} . Values >16 are hatched.

variations, whereas it is around 70%–80% over most land areas except for deserts and high terrain such as the Tibetan Plateau and the Rocky Mountains, where RH is low (e.g., 30%–50% in summer). Over most inland areas, RH is considerably lower in JJA than in DJF by 5%–20% (Fig. 4), mainly because the increases of the saturation vapor pressure associated with summer warm temperatures is larger than the increases in actual q . Our mean RH is slightly (by 1%–3%) lower than that for 1973–86 of Peixoto and Oort (1996) over the North Pacific and a few other oceanic areas. This is consistent with the decreasing RH trends discussed below.

Figure 5 shows that JJA surface RH is about 10%–15% higher at night than during the day over most of

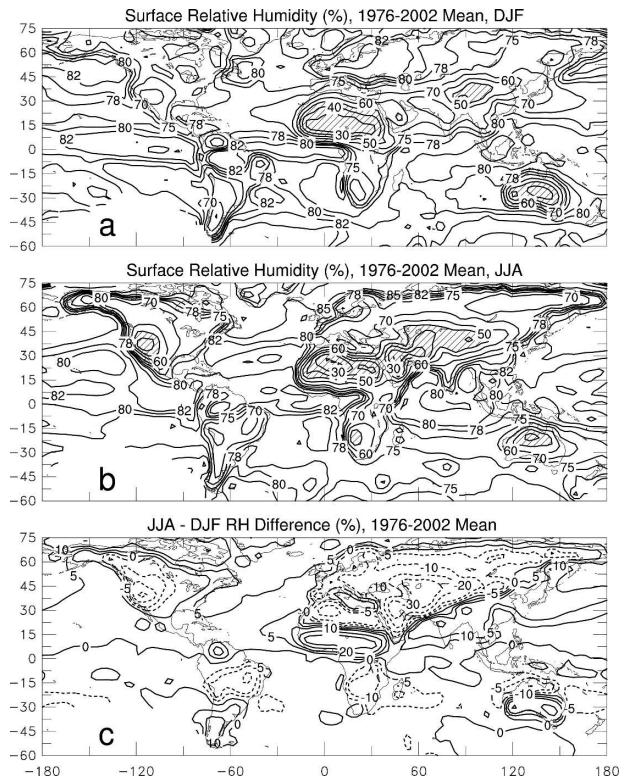


FIG. 4. Long-term (1976–2002) mean surface RH (%) derived from surface observations for (a) DJF, (b) JJA, and (c) DJF minus JJA difference. Contour levels are 10%, 20%, ..., 60%, 70%, 75%, 78%, 80%, 82%, 85%, and 90% with values $<50\%$ being hatched in (a) and (b), and 0%, $\pm 5\%$, $\pm 10\%$, $\pm 20\%$, $\pm 30\%$, and $\pm 40\%$ with negative values in dashed lines in (c).

the continents. This night–day difference decreases to 1%–5% in DJF at northern mid- and high latitudes, and it is small ($\sim 0\%$ – 2%) over the oceans. Surface q is slightly larger (by 0.2 – 0.5 g kg^{-1}) during daytime than nighttime over low-latitude oceans, and the night–day q difference is very small ($<0.25 \text{ g kg}^{-1}$) over the rest of the globe (not shown). Thus, the night–day RH difference is caused by diurnal variations in saturation vapor pressure induced by the large diurnal cycle in surface air temperature over land (Dai and Trenberth 2004). The night–day RH difference over the United States in Fig. 5 is similar to that shown by Gaffen and Ross (1999). We note that the night–day mean difference shown in Fig. 5 is smaller than the diurnal maximum–minimum amplitude.

The standard deviation (s.d.) of year-to-year variations of q is around 0.6 – 1.0 g kg^{-1} ($\sim 3\%$ – 5% of the mean) at low latitudes and 0.2 – 0.6 g kg^{-1} ($\sim 8\%$ – 15% of the mean) at mid and high latitudes, while the s.d. of RH is around 2%–4% over most of the globe (Fig. 6). The s.d. of both q and RH has relatively small spatial and seasonal variations.

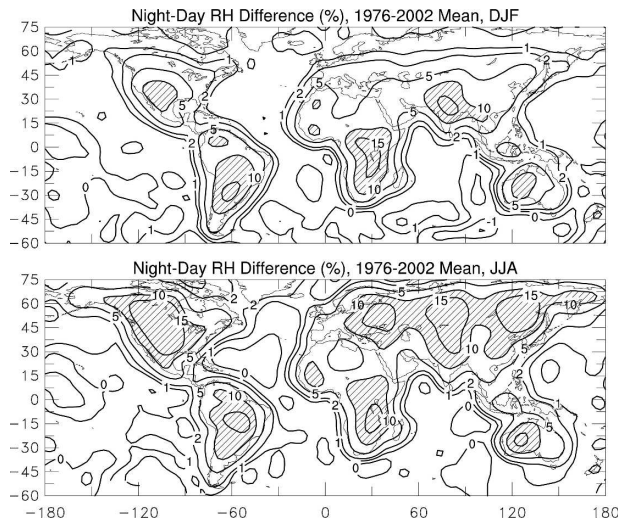


FIG. 5. Nighttime (6 P.M.–6 A.M.) minus daytime (6 A.M.–6 P.M.) RH difference (%), 1976–2002 mean) for (top) DJF and (bottom) JJA. Contour levels are $\pm 1\%$, $\pm 2\%$, 5%, 7%, 10%, 15%, and 20%.

The relatively invariant RH over the oceans suggests that marine surface air tends to reach a certain level ($\sim 75\%$ – 85%) of saturation with respect to water vapor. Atmospheric vertical and horizontal mixing likely plays an important role in maintaining the RH distribution, but it is unclear what exactly determines this saturation level, the spatial homogeneity, and the temporal invariance of marine RH. Over land, however, surface RH shows large spatial, diurnal and seasonal variations.

An EOF analysis (of the correlation matrix of the annual data) revealed some distinguishable patterns of variation for q and RH during 1976–2004. Figure 7 shows that the two leading principal components (PCs) of q (black line) and T (red line) are highly correlated, which confirms the dominant influence of T on q . The first EOF of q , which accounts for $\sim 18\%$ of the total variance, represents an upward trend embedded with considerable year-to-year variations, with the largest contribution from Asia and the Atlantic Ocean. This trend pattern is discussed further in the next section. The second EOF ($\sim 10\%$ variance) correlates with the El Niño–Southern Oscillation (ENSO) both in time and space, suggesting that surface temperature variations associated with ENSO have considerable influences on global surface q , especially over the Pacific and Indian Oceans (Fig. 7). However, ENSO's influence is not evident in surface RH, whose leading PC/EOF shows a secular trend over many oceanic areas (negative) and some land areas (positive; Fig. 7) but no ENSO-related patterns. The eigenvalues of the EOFs shown in Fig. 7 are statistically significant or separable.

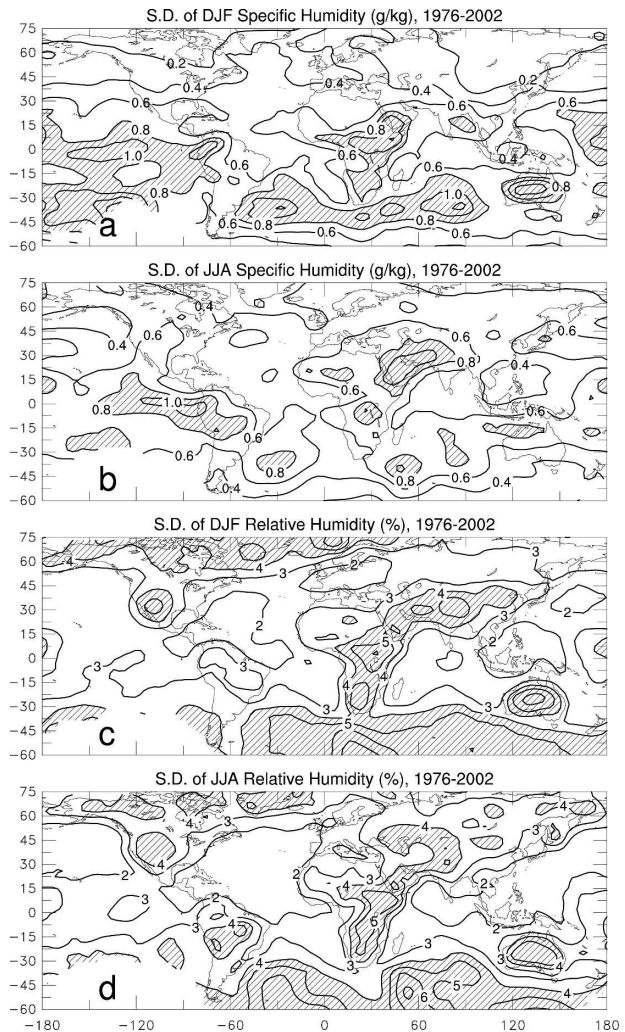


FIG. 6. Standard deviation of (a) DJF and (b) JJA surface specific humidity (g kg^{-1}), and standard deviation of (c) DJF and (d) JJA surface RH (%) during 1976–2002. Hatching indicates values $>0.8 \text{ g kg}^{-1}$ in (a) and (b), and $>4\%$ in (c) and (d).

4. Trends in surface humidity

a. Relative humidity trends

Figure 8 shows the global and hemispheric time series of annual RH averaged over all (black solid line), ocean (dashed line), and land (thin solid line) areas within 60°S – 75°N from 1976 to 2004. The RH changes are small (within 0.6%) compared with their mean values (about 74% , 79% , and 65% for the globe, ocean, and land, respectively). Nevertheless, decreasing trends [-0.11% to -0.22% (of saturation) decade^{-1}] over the global and hemispheric oceans are statistically significant (Fig. 8). A downward trend ($-0.20\% \text{ decade}^{-1}$, $p = 1.81\%$) is also evident in the Southern Hemisphere land+ocean time series. Over Northern Hemisphere land, the trend is positive but small and insignificant.

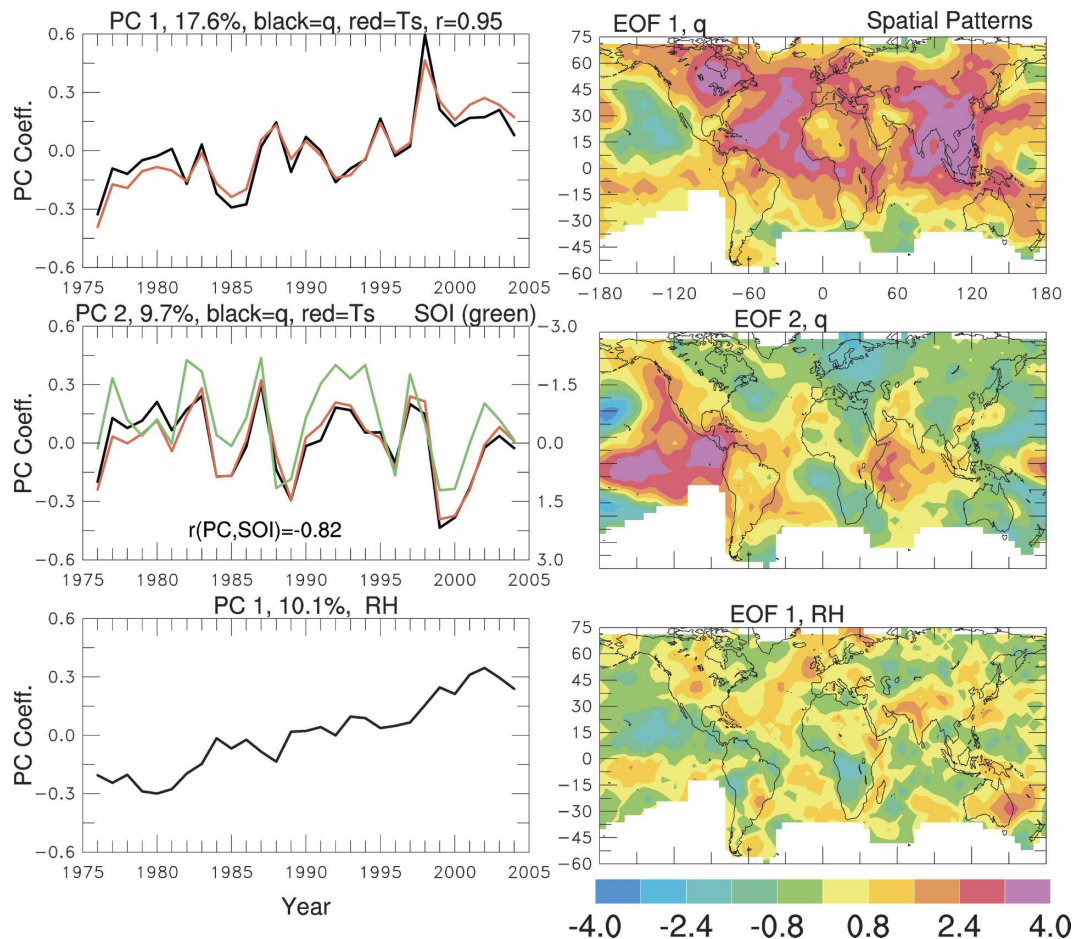


FIG. 7. (top), (middle) Leading (left) PCs of annual surface specific humidity (black) and air temperature (red) and (right) EOFs of the specific humidity. The percentage variance explained by the humidity PC/EOF is shown on top of each left panel (it is 20.7% and 12.0% for the temperature EOF 1 and 2, respectively). Also shown with the PC2 is the annual Southern Oscillation index (SOI; green curve, increases downward on the right ordinate), which has a correlation coefficient of -0.82 with the humidity PC. (bottom) The first PC and EOF of annual surface RH.

Consistent with the area-averaged time series, decreasing RH trends of 0% to -1% decade $^{-1}$ are widespread over the oceans (Fig. 9c). Large positive and statistically significant RH trends ($0.5\% \sim 2.0\%$ per decade) are seen over the central and eastern United States, India, and western China (Fig. 9c), and they exist in all four seasons (but largest in JJA over the central United States; not shown). From 1976 to 2004, RH also has increased over most of East Asia, but decreased over eastern Australia and eastern Brazil (Fig. 9c). The RH trend patterns are significantly correlated with those of surface specific humidity but not temperature (Fig. 9).

Figure 10 shows that the large RH increases over the central United States and India are accompanied with large upward trends in surface q and total cloud cover. The cloud data in Fig. 10 were derived from the same

synoptic reports as q and RH, except for the United States, where automated cloud observations after 1993 at most of the U.S. weather stations are not comparable with previous records, and we had to use the human cloud observations from ~ 124 U.S. military weather stations for 1994–2004 (see Dai et al. 2006 for details). The recent increase in U.S. cloudiness is a continuation of an upward trend started in the 1940s (e.g., Dai et al. 1999), and it is physically consistent with another independent record of diurnal temperature range (Dai et al. 2006). Since the warming is moderate over the central United States (cooling in JJA; not shown; see also Hansen et al. 2001) and India and western China (Fig. 9a), the large q increases exceeded those in saturation humidity and resulted in the RH increases in these regions. The increase in cloud cover (mostly for low clouds; not shown) suggests that the surface RH in-

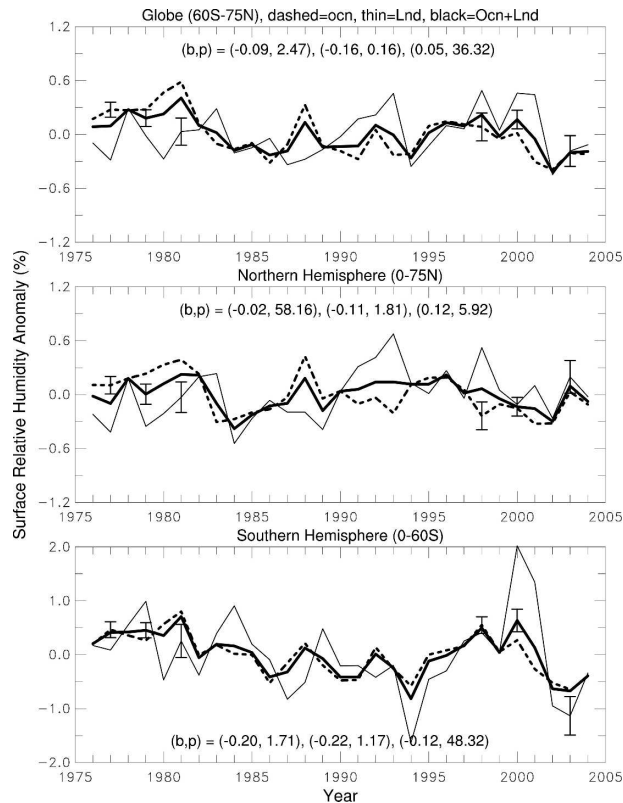


FIG. 8. Time series of annual-mean surface RH anomalies (%) averaged over global (60°S–75°N) and hemispheric land (thin solid line), ocean (dashed line), and land+ocean (thick solid line). Also shown are the pairs of the linear trend (b , % decade⁻¹) and its statistical significance (p , in %, $p < 5\%$ would be significant at the 5% level) for the land+ocean, ocean, and land curves from left to right. The error bars are estimated \pm standard error ranges based on spatial variations.

crease extended to the lower troposphere. The strong correlations among the physically related variables shown in Fig. 10 suggest that the data are consistent with each other and the upward trends are real.

b. Specific humidity trends

Figure 11 compares the global (60°S–75°N) and hemispheric time series of annual q (solid line) and T (short-dashed line). The T time series were derived from land air temperature and SST from the same surface synoptic reports as q , and they are very similar to the quality-controlled HadCRUT2 temperature data (long-dashed line in Fig. 11). The small discrepancies between these two temperature estimates result from differences in (temporal and spatial) sampling and analysis methods. Since q is derived from independent measurements of P_s and T_d [cf. Eq. (1)] and because of the dominant control of T on q as discussed above, the

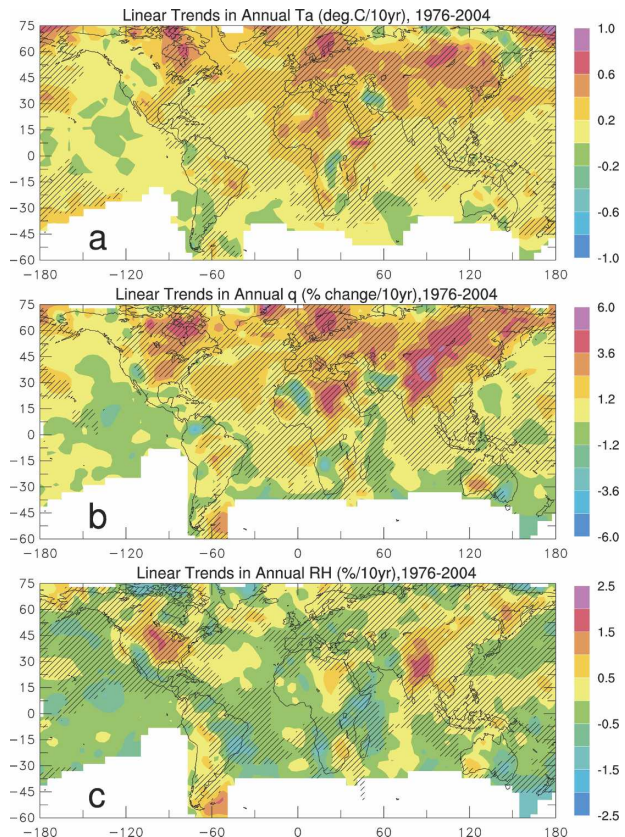


FIG. 9. Spatial distributions of linear trends during 1976–2004 in annual-mean surface (a) temperature [$^{\circ}\text{C} (10\text{yr})^{-1}$], (b) specific humidity [% change $(10\text{yr})^{-1}$], and (c) RH [% $(10\text{yr})^{-1}$]. The spatial patterns are correlated between (a) and (b) ($r = 0.39$, lower if the q trend is not normalized by its mean) and between (b) and (c) ($r = 0.62$). Hatching indicates the approximate areas where trends are statistically significant at the 5% level.

strong correlation between the q and T time series (Fig. 11) suggests that both the q and T data are likely reliable.

Global and Northern Hemispheric time series of both q and T (Fig. 11) show large and statistically very significant upward trends from 1976 to 2004 (excluding 1976 still yielded significant trends). Surface humidity increased by $\sim 0.06\text{ g kg}^{-1}\text{ decade}^{-1}$ globally and 0.08 g/kg per decade in the Northern Hemisphere during 1976–2004, while surface air temperature rose by $\sim 0.16^{\circ}\text{C decade}^{-1}$ globally and $0.20^{\circ}\text{C decade}^{-1}$ in the Northern Hemisphere during the same period. Southern Hemispheric q trend is positive but small and statistically insignificant (note that some areas have no data; cf. Fig. 2), although the T trend is significant (but insignificant when marine air temperature is used; not shown). Considerable interannual variations in q closely follow those in T . For example, record-breaking

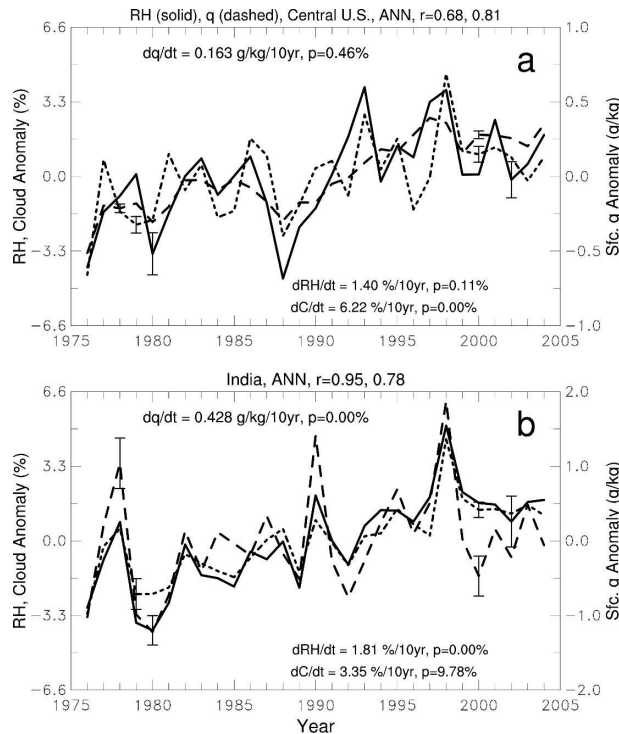


FIG. 10. Anomaly time series of annual surface RH (solid line), q (short-dashed line), and total cloud cover (long-dashed line) averaged over (a) the central United States (34°–44°N, 84°–104°W) and (b) India (10°–30°N, 74°–88°E) from 1976 to 2004. The correlation coefficient (r) between RH and q and between RH and cloud cover is shown on top of the panels from left to right. The slope and its statistical significance (p) are also shown (dC/dt for cloud cover slope). The cloud cover in (a) was divided by a factor of 4 before plotting. The error bars are estimated \pm standard error ranges based on spatial variations.

high temperatures in 1998 resulted in the highest q during 1976–2004.

Trends in nighttime (6 P.M.–6 A.M. local solar time) mean q and T are larger than those of daytime (6 A.M.–6 P.M.) over land (Fig. 12). This is consistent with a decreasing diurnal temperature range (DTR) over many land areas resulting from larger warming in the nighttime minimum temperature than in the daytime maximum temperature (e.g., Easterling et al. 1997; Dai et al. 1999, 2006). Over the oceans, the day–night differences in q and T trends are very small (not shown).

The time series of many regional q and T also show increasing trends and strong correlation between them. For example, Fig. 13 shows that annual q and T averaged over the contiguous United States, western Europe (west of 30°E), and central Eurasia (40°–60°N, 30°–100°E) has increased by 0.101, 0.130, and 0.125 g kg^{−1}, respectively, from 1976 to 2004. Accompanying these positive humidity trends, surface air temperature has also increased over these regions. The contiguous

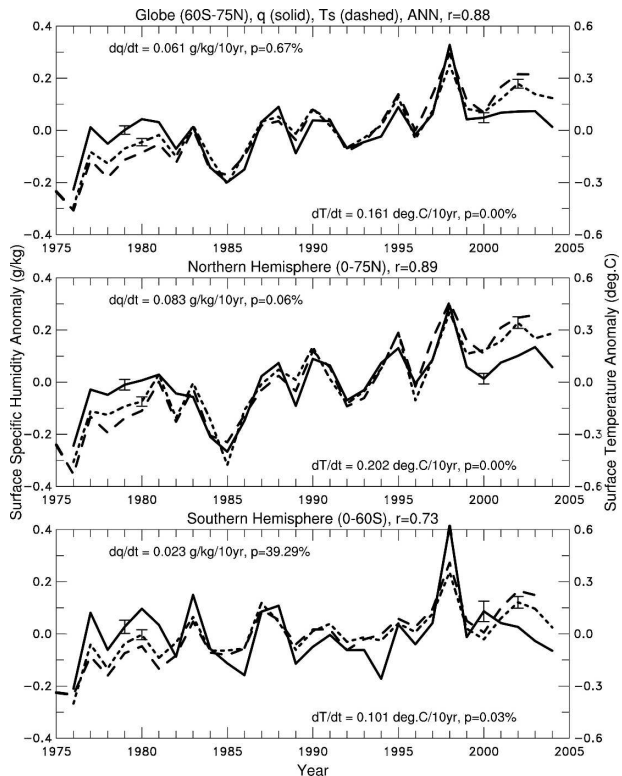


FIG. 11. Time series of annual-mean surface specific humidity (g kg^{−1}, solid curve) and surface (air over land and sea surface over oceans) temperature (°C, short-dashed curve) anomalies averaged over the globe (60°S–75°N), Northern Hemisphere (0°–75°N), and Southern Hemisphere (0°–60°S). The correlation coefficient (r) and the linear trends (dq/dt and dT/dt) and their statistical significant levels (p) are also shown. The error bars are estimated \pm standard error ranges based on spatial variations. Also shown (long-dashed curve) is the surface (air over land and sea surface over oceans) temperature based on the HadCRUT2 dataset (Jones and Moberg 2003; Rayner et al. 2003).

U.S. warming trend is, however, statistically insignificant, and its q – T correlation is noticeably lower than the other regions (Fig. 13). The relatively small warming over the United States (mainly due to cooling in summer) has been noticed before (e.g., Hansen et al. 2001).

There exists a significant correlation ($r = 0.39$, and 0.46 if marine air temperature is used) between the trend patterns of q and T (Figs. 9a–b). For example, large warming ($\sim 0.2^\circ$ – 0.7° C decade^{−1}) occurred over much of Eurasia, where surface q also shows the largest percentage increases (by 1.5%–6.0% decade^{−1}). Warming is also widespread over Africa, eastern North America, Mexico, and the Atlantic, North Pacific, and Indian Oceans, where surface humidity also generally increased (by 0%–2.5% decade^{−1}). The T and q trends over most of these regions are statistically significant at a 5% level (not shown). The q trend over the oceans in

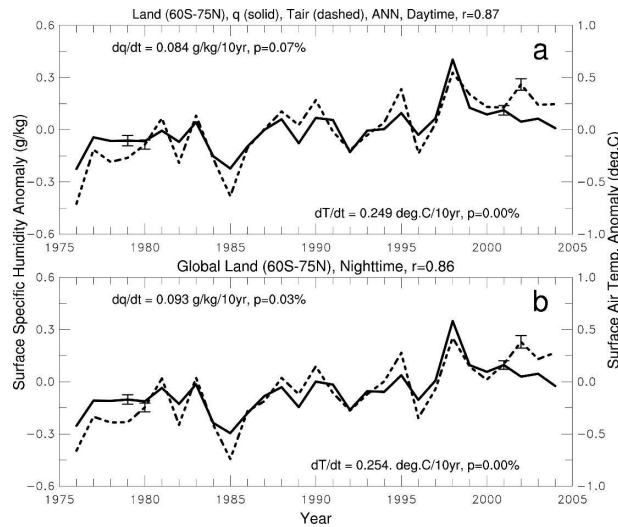


FIG. 12. Same as in Fig. 11, but for (top) daytime (6 A.M.–6 P.M.) and (bottom) nighttime (6 P.M.–6 A.M.) mean surface specific humidity (solid curve) and temperature (dashed curve) averaged over global (60°S–75°N) land areas.

the Southern Hemisphere is small and statistically insignificant, and it is slightly negative (statistically insignificant) over the tropical eastern Pacific Ocean (Fig. 9b).

The increasing humidity trends and their association with surface warming (mainly over the Northern Hemisphere) are found in all seasons, although the q – T correlation is higher in JJA than DJF (Fig. 14). The magnitude of the q trends is also larger in JJA than DJF, despite the larger DJF warming in the Northern Hemisphere. This is mainly owing to the higher mean q in JJA over land. The seasonal trends of q and T over the Southern Hemisphere are also positive, but generally small and statistically insignificant. Warming and increasing q are seen in all seasons over much of Eurasia and the Atlantic Ocean, but they are particularly large in DJF over Eurasia and the United States (not shown) whereas some cooling and q decreases have occurred in March–May (MAM) over Canada and the northern United States and in DJF over northern Siberia (not shown).

The recent warming and the associated surface humidity increases are broadly captured by the PCM when forced with realistic forcing (Fig. 15). Although the global and hemispheric time series of q and T differ slightly among the individual ensemble runs (not shown), they all exhibit upward trends and strong q – T correlations that are comparable to observations. However, the PCM overestimates the volcanic cooling effects (in 1982 and 1991) and underestimates the year-to-year variations in other years, resulting in stronger

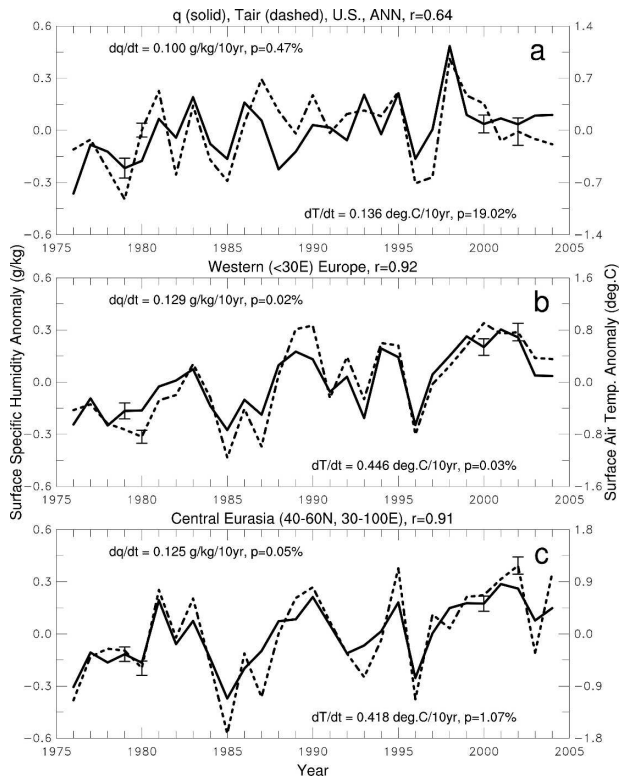


FIG. 13. Same as in Fig. 11, but for (a) the contiguous United States, (b) western (<30°E) Europe, and (c) central Eurasia (40°–60°N, 30°–100°E).

q – T correlation than observed (cf. Figs. 11 and 15). The model also overestimates the increases in Southern Hemispheric q and T a, while the increasing trends over the Northern Hemisphere are very similar to observations. Spatial trend patterns of T and q vary among the individual ensemble runs on regional scales (not shown), but they generally larger over the northern mid- and higher latitudes than in low latitudes, and the T and q trend patterns are correlated with each other, which is consistent with observations. More thorough analyses of the simulated humidity fields from the PCM and other coupled climate models are needed.

c. Humidity–temperature relationship

Because atmospheric water vapor provides a strong positive feedback to greenhouse gas–induced global warming, a realistic q – T relationship is vital for climate models to correctly simulate future climate change. Several studies have examined the relationship between tropospheric water vapor content and surface air temperature in observations (often based on sparse radio soundings) and models (e.g., Gaffen et al. 1992, 1997; Sun and Oort 1995; Sun and Held 1996; Ross et al.

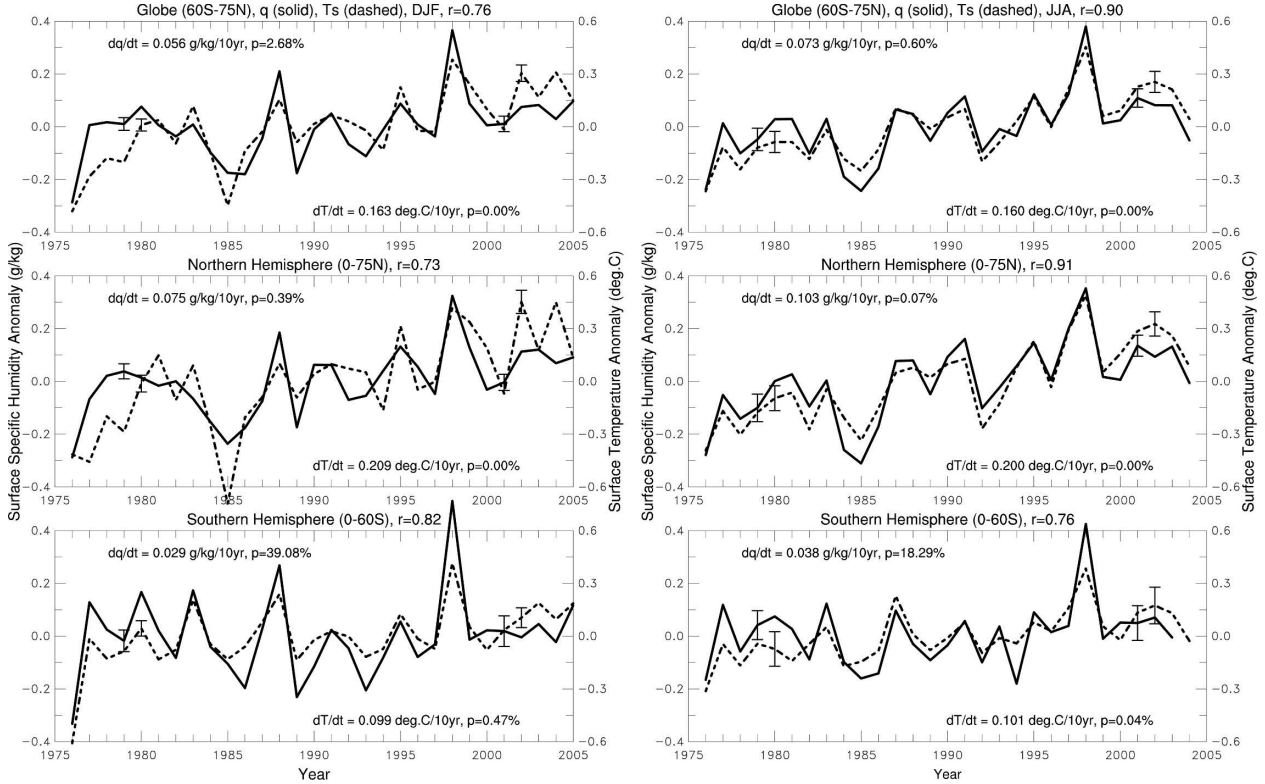


FIG. 14. Same as in Fig. 11, but for (left) DJF and (right) JJA seasons.

2002). For example, Gaffen et al. (1992) found that observed atmospheric PW relates to surface air temperature (T) through $\ln(\text{PW}) = A + BT$, but the coefficients A and B depend on T 's range. Sun and Oort (1995) and Sun and Held (1996) found that the observed rate of fractional increase of tropospheric q with temperature is significantly smaller than that given by the Geophysical Fluid Dynamics Laboratory (GFDL) model with constant RH; however, this result is found by Bauer et al. (2002) to be mostly an artifact of the sparse oceanic sampling by radiosondes and the objective analysis used by Sun and Oort (1995). Recently, Trenberth et al. (2005) show that atmospheric PW increases with surface T at a rate consistent with fairly constant RH over the oceans during the last two decades.

We showed in section 4a that area-averaged surface q and T are highly correlated on both interannual and longer time scales. Here we explore the surface q - T relationship in more detail. Figure 16 shows the scatterplots of globe (60°S-75°N), global land, and ocean-averaged annual q and T anomalies and compare the observed q - T relationship with estimates based on a constant humidity. Note that the constant humidity anomaly estimates (dashed lines) in Fig. 16 were derived using small T changes and globally averaged

mean surface air temperature, pressure, and relative humidity [and Eq. (3) and the e - q relationship]. Nevertheless, Fig. 16 shows that the dq - dT anomaly relationship is approximately linear [consistent with Eq. (3) for small dT], and the observed dq/dT is close to the constant RH slopes, suggesting that changes in global-mean annual RH during 1976-2004 are small (consistent with Figs. 8 and 9c). The observed dq/dT is about 0.58, 0.38, and 0.77 $\text{g kg}^{-1} \text{ } ^\circ\text{C}^{-1}$ ($r^2 = 0.81, 0.77$, and 0.76) for annual q and T for the globe, global land, and ocean, respectively. In percentage terms, they are about 4.9%, 4.3%, and 5.7% change in q per 1°C warming, which are close to those ($\sim 5.4\%$, 5.1% , and 5.5% per 1°C , respectively) suggested by the Clausius-Clapeyron equation or its empirical version [Eq. (3)] for saturation specific humidity (computed locally and then area averaged).¹

Figure 17 shows the scatterplot of annual global-mean q and T anomalies from the four ensemble runs

¹ The Clausius-Clapeyron equation locally gives 6.2%-6.4% change per 1°C in surface saturation specific humidity (q_s) for air temperature within 15° - 20°C . For regional averages, however, this percentage is lower because the area-averaged mean q_s is higher than that calculated using the Clausius-Clapeyron equation and area-averaged mean air temperature and pressure.

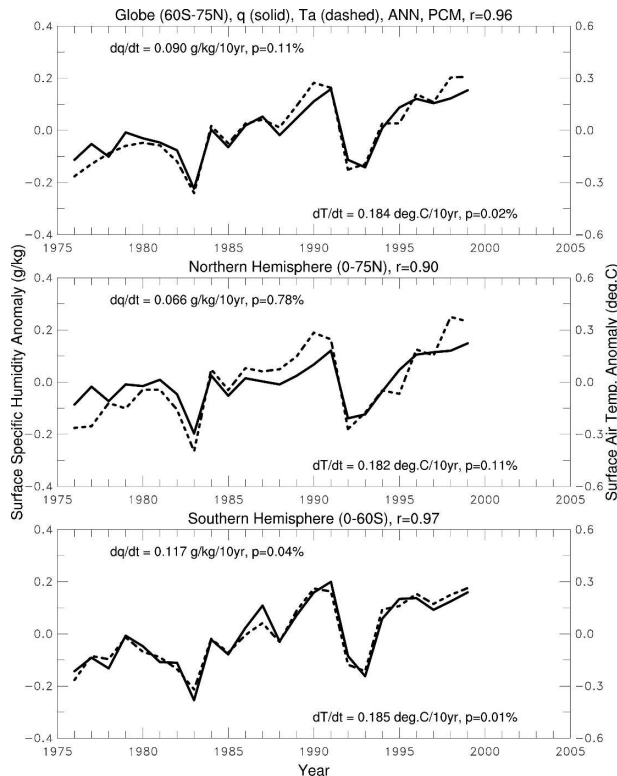


FIG. 15. Same as in Fig. 11, but for surface specific humidity and air temperature from one ensemble run by a coupled climate system model (i.e., PCM) using observation-based forcing of greenhouse gases, sulfate and volcanic aerosols, ozone, and solar radiation changes.

(donated by different symbols) by the PCM during the 1976–99 period. In this model, which has a cold global-mean bias of $\sim 2^{\circ}\text{C}$, the global-mean q increases linearly with surface temperature at a rate of 0.52 g kg^{-1} or about $5\% (1^{\circ}\text{C})^{-1}$ ($r^2 = 0.90$), which are comparable to those observed [0.58 g kg^{-1} or $4.9\% (1^{\circ}\text{C})^{-1}$; cf. Fig. 16]. Obviously, the absolute q increase, which is important for the water vapor feedback, depends on the model mean q and thus T . The $dq-dT$ fit is slightly better in the PCM than in observations ($r^2 = 0.90$ versus 0.81), which suggests that the model is more constrained to an invariant RH than in the real world.

The strong surface $q-T$ correlation is also seen at individual locations (Fig. 18a). This is especially true over most of the oceans, with the annual $q-T$ correlation higher than 0.8 over most of the North Pacific, North Atlantic, and eastern tropical Pacific Ocean. The $q-T$ correlation is also relatively strong over most of Eurasia and North America ($r = 0.4-0.8$), whereas it is weak and statistically insignificant over deserts and arid areas, such as the western United States and northern Mexico, southern and northern Africa, the Middle

East, and most of Australia (Fig. 18a). In these dry regions, dry soils and atmospheric subsidence have large impacts on surface q , leading to weak surface $q-T$ correlation. The $q-T$ correlation is also weak over most of South America for reasons unclear.

In contrast to the generally strong $q-T$ relationship, the correlation between annual surface RH and T is weak and statistically insignificant over most of the globe (Fig. 18b), even though large diurnal RH variations are caused mostly by T variations (cf. Fig. 5). The RH- T correlation is negative over the dry areas mentioned above where the $q-T$ correlation is weak or negative. This is expected because surface evaporation over these regions is limited by soil wetness, and it often cannot meet atmospheric demand to maintain a constant RH as air temperature increases. This is also consistent with the strong RH- q correlation ($r > 0.6$) over these regions (Fig. 18c) because any increases in q (e.g., due to increased soil wetness from precipitation) should raise the local RH. As expected, the RH- q correlation is positive over most of the globe, although it is weak over the North Pacific, Europe and some other places. The $q-T$ and RH- T correlation over the United States and the tropical western Pacific is in general agreement with that of Ross et al. (2002).

5. Summary and concluding remarks

We have analyzed surface specific (q) and relative (RH) humidity calculated using weather reports of surface air and dewpoint temperatures and air pressure from over 15 000 stations (from NCAR DS464.0) and from ships (mainly from the ICOADS) over the globe from December 1975 to spring 2005. We first examined the climatology and variability and then the trends and their relationship with temperature increases. Data quality controls were applied to exclude random outliers from measurement, transmission, and other errors. No attempt was made to address systematic errors and biases caused by measurement changes as necessary metadata are unavailable. For example, ship height may increase as ships get bigger and this could affect the measured q and RH over the oceans, although ship height changes are relatively small during the last 30 yr compared with earlier decades. Considerable instrumental and sampling errors likely exist in the data, although the strong $q-T$ correlation suggests that the variations and changes in surface humidity reported here are likely to be real given that the T time series (e.g., those from CRU in Fig. 11) are well established. In addition, the magnitude of the humidity trends is sensitive to the time period considered, especially given the relatively short length of records. For comparison,

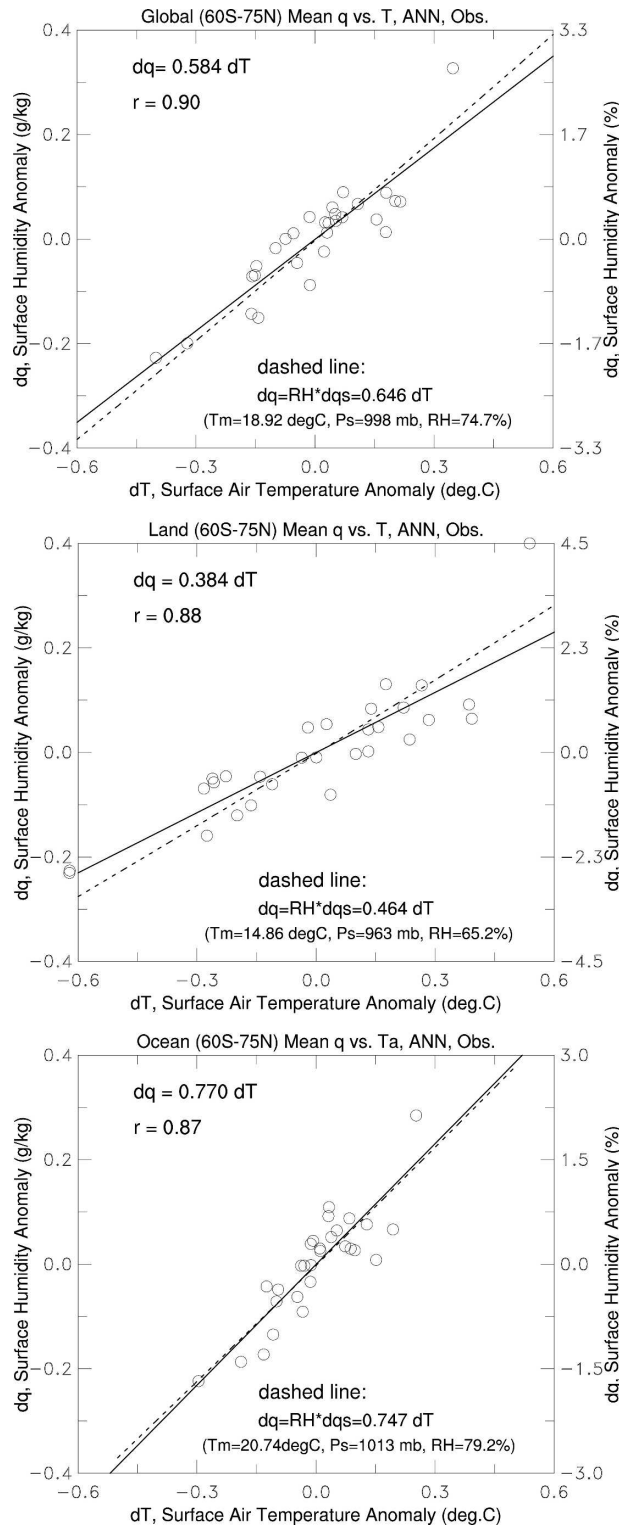


FIG. 16. Scatterplots of annual surface specific humidity (in units of g kg^{-1} and % of the mean) and surface air temperature ($^{\circ}\text{C}$) anomalies averaged over (top) all, (middle) land, and (bottom) ocean areas within 60°S – 75°N during 1976–2004. The solid line is the linear regression of all the data points (circles) while the dashed line is based on a constant mean RH and a saturation rate (the observed values of the mean state are shown in the parentheses).

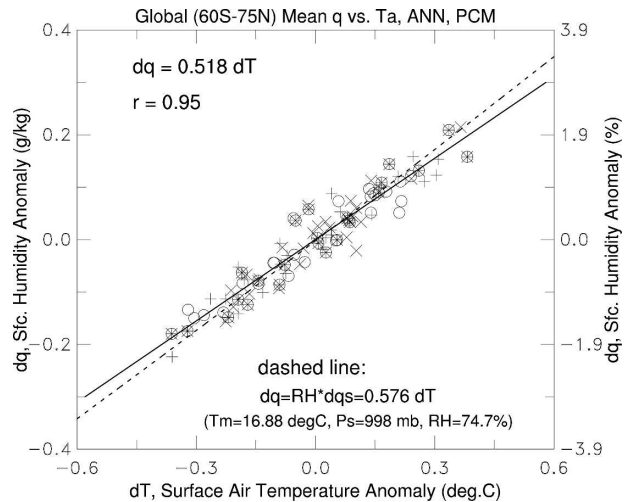


FIG. 17. Scatterplot of annual mean surface specific humidity (in units of g kg^{-1} and % of the mean) and air temperature ($^{\circ}\text{C}$) anomalies averaged over all areas within 60°S – 75°N from four ensemble simulations (denoted by different symbols) for the 1976–99 period using a coupled climate system model with realistic forcing. The solid line is the linear regression of all the data points while the dashed line is based on a constant mean RH and a saturation rate (the mean state values are shown in the parentheses).

we also analyzed the surface q and temperature (T) simulated by a fully coupled climate model (PCM) from 1976 to 1999 with realistic forcing. The main results are summarized below.

Spatial distributions of long-term mean surface q are largely controlled by climatological surface air temperature, with the largest q of 17 – 19 g kg^{-1} in the Tropics and large seasonal variations over northern mid- and high-latitude land. One exception is the subtropical land areas where atmospheric subsidence causes low surface q . Surface RH, on the other hand, has relatively small spatial and interannual variations; it is within 75% – 82% over most oceans during all seasons and within 70% – 80% over most land areas except for dry areas (e.g., northern Africa and inland Australia) and high terrain (e.g., the Rockies and Tibet) where surface RH is low (30% – 60%). Seasonal RH variations are small over the oceans, but considerable (5% – 30% ; lower in JJA) over many land areas. Nighttime RH is 2% – 15% higher than daytime RH over most land areas resulting from large temperature diurnal cycles, while the night–day difference is only about 1% over the oceans. The leading EOF in both the q and RH represents secular long-term trends, while the second EOF of q (but no EOF of RH) is related to ENSO with large positive q anomalies over the eastern tropical Pacific during El Niños.

During 1976–2004, global changes in surface RH are relatively small (within 0.6% ; absolute value), although

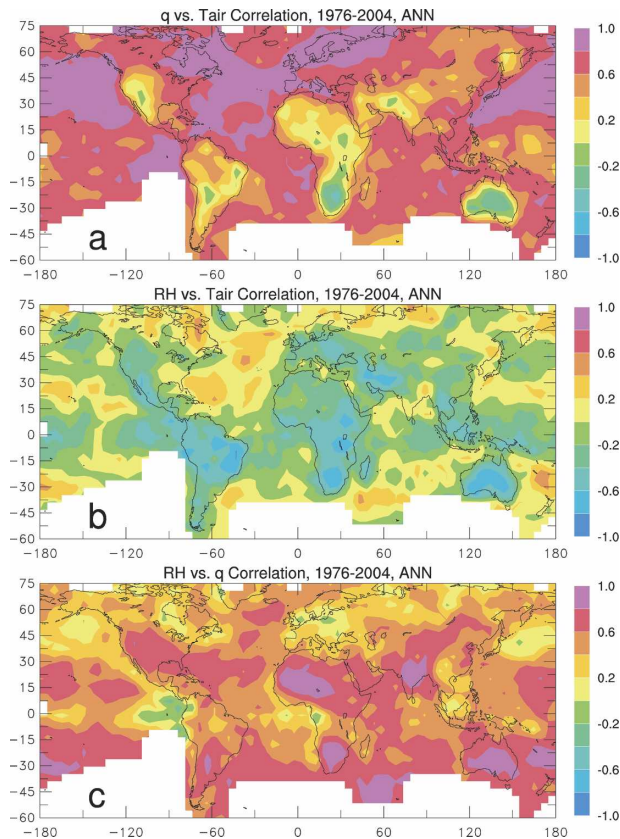


FIG. 18. Maps of correlation coefficients between observed annual mean surface (a) specific humidity and air temperature, (b) RH and air temperature, and (c) RH and specific humidity during 1976–2004. Values above (below) about $+0.4$ (-0.4) are statistically significant.

decreasing trends (-0.11% to -0.22% decade $^{-1}$) in the RH averaged over the global and hemispheric oceans are statistically significant. Decreasing RH trends of 0% to -1% decade $^{-1}$ are widespread over the oceans, but locally these trends are statistically significant only over most of the North Pacific and tropical eastern Pacific Ocean. Large positive and statistically significant RH trends ($0.5\% \sim 2.0\%$ decade $^{-1}$) are seen over the central and eastern United States, India, and western China in all seasons, and these RH increases are accompanied by upward trends in surface q and total and low cloud cover. The RH increases resulted from large q increases that exceeded those in saturation humidity (associated with moderate warming) and caused the RH to rise in these regions. The cloud cover change suggests that the surface RH increase extended to the lower troposphere.

Statistically very significant increasing trends are found in global and Northern Hemispheric q and T . From 1976 to 2004, annual surface q (T) increased by 0.06 g kg^{-1} (0.16°C) decade $^{-1}$ globally and 0.08 g kg^{-1}

(0.20°C) decade $^{-1}$ in the Northern Hemisphere, while trends in Southern Hemispheric q are positive but statistically insignificant. Over land, the q and T trends are larger at night than during the day, consistent with a decreasing diurnal temperature range observed over many land areas. The largest percentage increases in surface q (by $1.5\% \sim 6.0\%$ decade $^{-1}$) have occurred over Eurasia where large surface warming ($\sim 0.2^\circ \sim 0.7^\circ\text{C}$ decade $^{-1}$) is also seen during 1976–2004. The increasing q trends and their association with surface warming exist in all seasons over much of Eurasia (largest in DJF) and the Atlantic Ocean.

Strong surface q – T correlation is found over most oceans ($r = 0.6 \sim 0.9$) and most of Eurasia and North America ($r = 0.4 \sim 0.8$), whereas it is weak and statistically insignificant over deserts and arid areas where atmospheric subsidence and soil wetness play an important role. Globally, the q – T anomaly relationship is approximately linear, and the observed dq/dT is close to the estimated rates using a constant RH. In percentage terms, surface q averaged over the globe, global land, and global ocean increases by 4.9% , 4.3% , and 5.7% per 1°C warming, respectively, values that are close to those suggested by the Clausius–Clapeyron equation with a constant RH.

The recent q and T trends are broadly captured by the PCM forced with realistic forcing. However, the model overestimates the volcanic cooling effects and underestimates the year-to-year variations in other years, resulting in stronger q – T correlation than observed. The model also overestimates the increases in Southern Hemispheric q and T .

The results of this study are consistent with previous analyses (see introduction) that showed increasing trends in surface humidity variables over a number of regions. The strong correlation between surface q and T on both interannual and longer time scales (including the trends) suggests that the increasing trends in global q will continue as global temperature rises. The exact rate of q increases differs spatially; however, globally it is close to that suggested by the Clausius–Clapeyron equation with a constant RH. Although global changes in surface RH are generally small, they may increase substantially on regional scales, as seen over the central and eastern United States, India, and western China, and the RH increases may be accompanied with increases in low cloudiness and decreases in DTR.

Acknowledgments. The author thanks Dian Seidel, Kevin Trenberth, and David Parker for constructive comments; Steve Running, Gregg Walters, and Steve Worley for helpful discussions on surface observations; and Warren Washington's group for making the PCM

simulations available. This study is partly supported by NCAR's Water Cycle Program.

REFERENCES

- Anderson, S. P., and M. F. Baumgartner, 1998: Radiative heating errors in naturally ventilated air temperature measurements made from buoys. *J. Atmos. Oceanic Technol.*, **15**, 157–173.
- Bauer, M., A. D. Del Genio, and J. R. Lanzante, 2002: Observed and simulated temperature–humidity relationships: Sensitivity to sampling and analysis. *J. Climate*, **15**, 203–215.
- Berry, D. I., E. C. Kent, and P. K. Taylor, 2004: An analytical model of heating errors in marine air temperatures from ships. *J. Atmos. Oceanic Technol.*, **21**, 1198–1215.
- Bolsenga, S. J., 1965: The relationship between total atmospheric water vapor and surface dew point on a mean daily and hourly basis. *J. Appl. Meteor.*, **4**, 430–432.
- Bolton, D., 1980: Computation of equivalent potential temperature. *Mon. Wea. Rev.*, **108**, 1046–1053.
- Brock, F. V., Ed., 1984: Instructor's handbook on meteorological instrumentation. NCAR Tech. Note NCAR/TN-237+IA, NCAR, Boulder, CO, 339 pp.
- , and S. J. Richardson, 2001: *Meteorological Measurement Systems*. Oxford University Press, 290 pp.
- Changnon, D., M. Sandstrom, and C. Schaffer, 2003: Relating changes in agricultural practices to increasing dew points in extreme Chicago heat waves. *Climate Res.*, **24**, 243–254.
- Cubasch, U., and Coauthors, 2001: Projections of future climate change. *Climate Change 2001: The Scientific Basis*, J. T. Houghton et al., Eds., Cambridge University Press, 525–582.
- Dai, A., 2001a: Global precipitation and thunderstorm frequencies. Part I: Seasonal and interannual variations. *J. Climate*, **14**, 1092–1111.
- , 2001b: Global precipitation and thunderstorm frequencies. Part II: Diurnal variations. *J. Climate*, **14**, 1112–1128.
- , and C. Deser, 1999: Diurnal and semidiurnal variations in global surface wind and divergence fields. *J. Geophys. Res.*, **104**, 31 109–31 125.
- , and J. H. Wang, 1999: Diurnal and semidiurnal tides in global surface pressure fields. *J. Atmos. Sci.*, **56**, 3874–3891.
- , and K. E. Trenberth, 2004: The diurnal cycle and its depiction in the Community Climate System Model. *J. Climate*, **17**, 930–951.
- , —, and T. R. Karl, 1999: Effects of clouds, soil moisture, precipitation, and water vapor on diurnal temperature range. *J. Climate*, **12**, 2451–2473.
- , G. A. Meehl, W. M. Washington, T. M. L. Wigley, and J. M. Arblaster, 2001: Ensemble simulation of twenty-first century climate changes: Business-as-usual versus CO₂ stabilization. *Bull. Amer. Meteor. Soc.*, **82**, 2377–2388.
- , T. R. Karl, B. Sun, and K. E. Trenberth, 2006: Recent trends in cloudiness over the United States: A tale of monitoring inadequacies. *Bull. Amer. Meteor. Soc.*, **87**, 597–606.
- Déry, S. J., and M. Stieglitz, 2002: A note on surface humidity measurements in the cold Canadian environment. *Bound.-Layer Meteor.*, **102**, 491–497.
- Easterling, D. R., and Coauthors, 1997: Maximum and minimum temperature trends for the globe. *Science*, **277**, 364–367.
- Elliott, W. P., 1995: On detecting long-term changes in atmospheric moisture. *Climate Change*, **31**, 349–367.
- Gaffen, D. J., and R. J. Ross, 1999: Climatology and trends of U.S. surface humidity and temperature. *J. Climate*, **12**, 811–828.
- , W. P. Elliott, and A. Robock, 1992: Relationships between tropospheric water-vapor and surface-temperature as observed by radiosondes. *Geophys. Res. Lett.*, **19**, 1839–1842.
- , R. D. Rosen, D. A. Salstein, and J. S. Boyle, 1997: Evaluation of tropospheric water vapor simulations from the Atmospheric Model Intercomparison Project. *J. Climate*, **10**, 1648–1661.
- Groisman, P. Ya., R. W. Knight, T. R. Karl, D. R. Easterling, B. M. Sun, and J. H. Lawrimore, 2004: Contemporary changes of the hydrological cycle over the contiguous United States: Trends derived from in situ observations. *J. Hydrometeorol.*, **5**, 64–85.
- Hansen, J., A. Lacis, D. Rind, G. Russell, P. Stone, I. Fung, R. Ruedy, and J. Lerner, 1984: Climate sensitivity: Analysis of feedback mechanisms. *Climate Processes and Climate Sensitivity*, *Geophys. Monogr.*, Vol. 29, Amer. Geophys. Union, 130–163.
- , R. Ruedy, M. Sato, M. Imhoff, W. Lawrence, D. Easterling, T. Peterson, and T. Karl, 2001: A closer look at United States and global surface temperature change. *J. Geophys. Res.*, **106**, 23 947–23 963.
- Ishii, M., A. Shouji, S. Sugimoto, and T. Matsumoto, 2005: Objective analysis of SST and marine meteorological variables for the 20th century using the ICOADS and the Kobe collection. *Int. J. Climatol.*, **25**, 865–879.
- Jones, P. D., and A. Moberg, 2003: Hemispheric and large-scale surface air temperature variations: An extensive revision and an update to 2001. *J. Climate*, **16**, 206–223.
- Kaiser, D. P., 2000: Decreasing cloudiness over China: An updated analysis examining additional variables. *Geophys. Res. Lett.*, **27**, 2193–2196.
- Kent, E. C., and P. K. Taylor, 1996: Accuracy of humidity measurement on ships: Consideration of solar radiation effects. *J. Atmos. Oceanic Technol.*, **13**, 1317–1321.
- , R. J. Tiddy, and P. K. Taylor, 1993: Correction of marine air temperature observations for solar radiation effects. *J. Atmos. Oceanic Technol.*, **10**, 900–906.
- Liu, W. T., 1986: Statistical relation between monthly mean precipitable water and surface-level humidity over global oceans. *Mon. Wea. Rev.*, **114**, 1591–1602.
- , W. Q. Tang, and P. P. Niiler, 1991: Humidity profiles over the ocean. *J. Climate*, **4**, 1023–1034.
- Meehl, G. A., W. M. Washington, C. Ammann, J. M. Arblaster, T. M. L. Wigley, and C. Tebaldi, 2004: Combinations of natural and anthropogenic forcings and twentieth-century climate. *J. Climate*, **17**, 3721–3727.
- New, M., M. Hulme, and P. Jones, 2000: Representing twentieth-century space–time climate variability. Part II: Development of 1901–96 monthly grids of terrestrial surface climate. *J. Climate*, **13**, 2217–2238.
- Norris, J. R., 2005: Multidecadal changes in near-global cloud cover and estimated cloud cover radiative forcing. *J. Geophys. Res.*, **110**, D08206, doi:10.1029/2004JD005600.
- Oort, A. H., 1983: Global atmospheric circulation statistics, 1958–1973. NOAA Prof. Paper 14, 180 pp. and 47 microfiche. [Available from author at GFDL/NOAA, P.O. Box 308, Princeton, NJ 08542.]
- Peixoto, J. P., and A. H. Oort, 1996: The climatology of relative humidity in the atmosphere. *J. Climate*, **9**, 3443–3463.
- Philippa, R., B. Durr, C. Marty, A. Ohmura, and M. Wild, 2004: Radiative forcing—Measured at Earth's surface—Corroborate the increasing greenhouse effect. *Geophys. Res. Lett.*, **31**, L03202, doi:10.1029/2003GL018765.
- Rayner, N. A., D. E. Parker, E. B. Horton, C. K. Folland, L. V.

- Alexander, D. P. Rowell, E. C. Kent, and A. Kaplan, 2003: Globally complete analyses of sea surface temperature, sea ice, and night marine air temperature since the late nineteenth century. *J. Geophys. Res.*, **108**, 4407, doi:10.1029/2002JD002670.
- Reitan, C. H., 1963: Surface dew point and water vapor aloft. *J. Appl. Meteor.*, **2**, 776–779.
- Robinson, P. J., 2000: Temporal trends in United States dew point temperatures. *Int. J. Climatol.*, **20**, 985–1002.
- Ross, R. J., and W. P. Elliott, 2001: Radiosonde-based Northern Hemisphere tropospheric water vapor trends. *J. Climate*, **14**, 1602–1612.
- , —, D. J. Seidel, and Participating AMIP-II Modeling Groups, 2002: Lower-tropospheric humidity–temperature relationships in radiosonde observations and atmospheric general circulation models. *J. Hydrometeorol.*, **3**, 26–38.
- Schönwiese, C. D., and J. Rapp, 1997: *Climate Trend Atlas of Europe Based on Observations 1891–1990*. Kluwer Academic, 228 pp.
- Shea, D. J., 1986: Climatological atlas: 1950–1979. NCAR Tech. Note NCAR TN-269+STR, 35 pp. and 154 figs. [Available from National Center for Atmospheric Research, P.O. Box 3000, Boulder, CO 80307.]
- Smith, W. L., 1966: Note on the relationship between total precipitable water and surface dew point. *J. Appl. Meteor.*, **5**, 726–727.
- Sun, B., P. Ya. Groisman, R. S. Bradley, and F. T. Keimig, 2000: Temporal changes in the observed relationship between cloud cover and surface air temperature. *J. Climate*, **13**, 4341–4357.
- Sun, D. Z., and A. H. Oort, 1995: Humidity–temperature relationships in the tropical troposphere. *J. Climate*, **8**, 1974–1987.
- , and I. M. Held, 1996: A comparison of modeled and observed relationships between interannual variations of water vapor and temperature. *J. Climate*, **9**, 665–675.
- Trenberth, K. E., J. G. Olson, and W. G. Large, 1989: A global ocean wind stress climatology based on ECMWF analyses. NCAR Tech. Note NCAR/TN-338+STR, 93 pp.
- , J. Fasullo, and L. Smith, 2005: Trends and variability in column-integrated atmospheric water vapor. *Climate Dyn.*, **24**, doi:10.1007/s00382-005-0017-4.
- van Wijngaarden, W. A., and L. A. Vincent, 2005: Examination of discontinuities in hourly surface relative humidity in Canada during 1953–2003. *J. Geophys. Res.*, **110**, D22102, doi:10.1029/2005JD005925.
- Wang, J. H., W. B. Rossow, and Y. C. Zhang, 2000: Cloud vertical structure and its variations from a 20-yr global rawinsonde dataset. *J. Climate*, **13**, 3041–3056.
- , H. L. Cole, D. J. Carlson, E. R. Miller, K. Beierle, A. Paukunen, and T. K. Laine, 2002: Corrections of humidity measurement errors from the Vaisala RS80 radiosonde—Application to TOGA COARE data. *J. Atmos. Oceanic Technol.*, **19**, 981–1002.
- Wang, J. X. L., and D. J. Gaffen, 2001: Late-twentieth-century climatology and trends of surface humidity and temperature in China. *J. Climate*, **14**, 2833–2845.
- Warren, S. G., C. J. Hahn, J. London, R. M. Chervin, and R. L. Jenne, 1988: Global distribution of total cloud cover and cloud type amounts over the ocean. NCAR Tech. Note TN-317+STR, 42 pp. and 170 maps.
- Washington, W. M., and Coauthors, 2000: Parallel climate model (PCM) control and transient simulations. *Climate Dyn.*, **16**, 755–774.
- Worley, S. J., S. D. Woodruff, R. W. Reynolds, S. J. Lubker, and N. Lott, 2005: ICOADS release 2.1 data and products. *Int. J. Climatol.*, **25**, 823–842.